Computational Modeling and Experimental Study on Optical Microresonators Using Optimal Spherical Structure for Chemical Sensing

Hanzheng Wang[1], Lei Yuan[1,2], Jie Huang[2], Xinwei Lan[2], Cheol-Woon Kim[3], Lan Jiang[2], Hai Xiao[*1]

[1]Department of Electrical and Computer Engineering, Missouri University of Science and Technology, School of Mechanical Engineering, [2]Beijing Institute of Technology, [3]MO-SCI Corporation
[1]Rolla, MO 65409, USA, [2]Beijing 100081, China, [3]Rolla, MO 65401, USA
[*]xiaoha@mst.edu

Abstract

Chemical sensors based on optical microresonators have been demonstrated highly sensitive by monitoring the refractive index (RI) changes in the surrounding area near the resonator surface. In an optical resonator, the Whispering Gallery Modes (WGMs) with high quality (Q) factor supported by the spherical symmetric structure interacts with the contiguous background through evanescent field. Highly sensitive detection can be realized because of the long lifetime of the photons. The computational models of solid glass microspheres and hollow glass spheres with porous wall (PW-HGM) were established. These two types of microresonators were studied through simulations. The PW-HGM resonator was proved as an optimal chemical sensor and verified by experiments and compared for chemical vapor detection. The simulation and experimental results agreed well in the sensing trends for PW-HGM microresonator.

Keywords

Whispering Gallery Modes; Microresonator; Computational Model; Simulation; Porous Wall; Chemical Sensor

Introduction

Substantial interests exist in chemical vapor sensing applications in various detection approaches (Crone et al., 2002; Wan et al., 2004; Wei, Dai, Roy& Tolle, 2006; Zamborini et al., 2002; Crone et al., 2001). Organic transistor based circuits can be employed for chemical vapor sensing and showed the improved sensing characteristics compared with discrete transistor based sensors (Crone et al., 2002; Crone et al., 2001). ZnO nanowires gas sensors were fabricated with micro electromechanical system and showed high sensitivity and fast response to ethanol gas at a working temperature of 300℃ (Wan et al., 2004). Also, a vertically aligned carbon material nanotube arrays as the sensing resources was applied to effectively enhance the sensitivity and broaden the choices of chemical gas analytes (Wei, Dai, Roy& Tolle, 2006). Electronic conductivity properties of network polymer films of Au_{140} nanoparticles were reported to allow for a swelling-induced modification in either length or chemical nature of electron channels at the presence of chemical vapor(Zamborini et al., 2002). Those approaches proved their chemical sensing ability when traditional electric based methods were applied (Crone et al., 2002; Wan et al., 2004; Wei, Dai, Roy& Tolle, 2006; Zamborini et al., 2002; Crone et al, 2001).

Optical sensing methods have been widely employed in chemical detection area with higher sensitivity and relatively faster response (Matsko & Ilchenko, 2006; Gregor et al., 2010; Homola, Yee &Gauglitz, 1999; Patrick, Kersey & Bucholtz, 1998; Wang et al., 2012). More recently, it has been noted that optical microresonator showed its capability for high sensitivity chemical detection (Matsko&Ilchenko, 2006; Gregor et al., 2010; Wang et al., 2012). Optical microresonator in spherical shape well utilizes its high-Q in Whispering Gallery Modes (WGMs) and fully extends its ability of long term interaction with chemical gas. The solid glass microsphere resonator was studies for their high detection limit and used for sensing gas vapors based on changes in thermal conductivity of the silica material when it interacts with the chemical vapors(Matsko & Ilchenko, 2006; Gregor et al., 2010). The structural variation on spherical resonators impacts their chemical sensing capability, such as the diversity of the microsphere wall structure (Matsko & Ilchenko, 2006; Gregor et al.,

2010; Wang et al., 2012). A porous wall hollow glass microsphere (PW-HGM) coupled with a single mode fiber taper was discussed for its sensing mechanism in various chemical vapors as the gas molecules enhanced the refractive index (RI) in the porous wall channels (Wang et al., 2012). The simulation modeling of WGMs has been studies on the electric field distribution confined with the surface of the microresonator (Wang et al., 2012; Teraoka & Arnold, 2006; Teraoka & Arnold, 2006; Teraoka & Arnold, 2003). For example, the solid glass microsphere WGMs have been theoretically discussed with a uniform surface or a dielectric coating layer in chemical vapor detection (Teraoka & Arnold, 2006; Teraoka & Arnold, 2006; Teraoka & Arnold, 2003).

The aim of our work was to theoretically explain the effect of different spherical resonator structures on chemical detection sensitivities and experimentally prove the simulation results. The computational model on the PW-HGM microresonator was presented and the comparison of its corresponding experimental results was shown.

Computational Modeling

WGM Modeling Theory

The structures and resonance spectra of the WGMs in excited microsphere resonators have been studied theoretically in recent years (Matsko & Ilchenko, 2006; Teraoka & Arnold, 2006; Teraoka & Arnold, 2006; Teraoka & Arnold, 2003; Lin et al., 2010). Generally, spherical coordinates are used to characterize the mode numbers in WGM: angular mode l, azimuthal mode m and radial mode v. Figure 1 demonstrates the models of WGMs in the solid glass microspheres and PW-HGM. The solid glass sphere model is shown in Figure 1 (a) with $n_0 = 1.0$and $n_s = 1.45$, and the PW-HGM model in Figure 1 (b) shows $n_s = n_0 = 1.0$ and $n_0 = 1.45$.

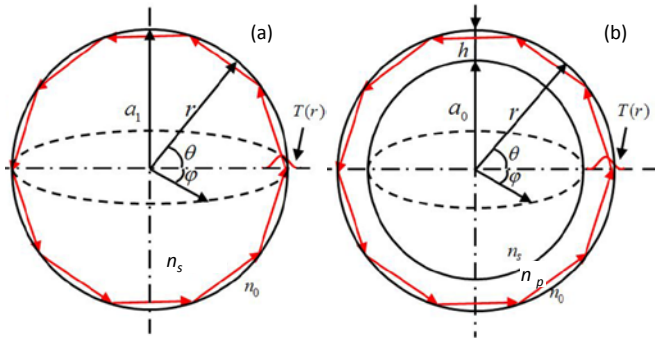

FIG. 1 WGM MODELS IN (a) SOLID GLASS SPHERE and (b) PW-HGM

The total internal reflection of light along the interface of microsphere wall and surroundings is shown in red arrowed lines in figure 1. The resonance wavelength λ_R can be expressed by the characteristic equation (Teraoka & Arnold, 2006; Teraoka & Arnold, 2006; Teraoka & Arnold, 2003; Lin et al., 2010):

$$\eta_s \frac{\chi_l'(n_0 k a_0)}{\chi_l(n_0 k a_0)} = \frac{\psi_l'(n_s k a_0)}{\psi_l(n_s k a_0)}$$

$$\eta_s = \begin{cases} \frac{n_0}{n_s}, & TEmodes \\ \frac{n_s}{n_0}, & TMmodes \end{cases} \quad (1)$$

Equation (1) is the characteristic equation of solid glass microsphere resonator. Functions ψ_l and χ_l are the spherical Ricatti-Bessel function and the spherical Ricatti-Neumann function, respectively.

TABLE 1 PARAMETERS OF SOLID GLASS MICROSPHERE AND PW-HGM MODELS

Microsphere types and parameters		
	Solid glass microsphere	**Porous wall hollow glass microsphere**
Diameter	a_0	$a_1 = a_0 + h$
Porous wall Thickness	0	h
Refractive index (RI)	$n_s = 1.45, n_0 = 1.0$	$n_p = 1.45, n_s = n_0 = 1.0$
Sensitivity	$(S_0)_{TE}, (S_0)_{TM}$	S_{TE}, S_{TM}
Wave vector (before RI change)	k_0	k_0
Electric field (before RI change)	T_0	T_0
Resonance wavelength	λ_R	λ_R

Resonant wave number is shown as $k = \frac{2\pi}{\lambda_R}$. The characteristic equation for PW-HGM can be expressed as (Teraoka & Arnold, 2006; Teraoka & Arnold, 2006; Teraoka & Arnold, 2003; Lin et al., 2010):

$$\eta_0 \frac{\chi_l'(n_0 k a_1)}{\chi_l(n_0 k a_1)} = \frac{B_l \psi_l'(n_p k a_1) + \chi_l'(n_p k a_1)}{B_l \psi_l(n_p k a_1) + \chi_l(n_p k a_1)}$$

$$B_l = \frac{\eta_p \psi_l'(n_s k a_0)\chi_l(n_p k a_0) - \psi_l(n_s k a_0)\chi_l'(n_p k a_0)}{\psi_l'(n_p k a_0)\psi_l(n_s k a_0) - \eta_p \psi_l(n_p k a_0)\psi_l(n_s k a_0)}$$

$$\eta_0 = \begin{cases} n_0/n_p, & TEmodes \\ n_p/n_0, & TMmodes \end{cases}$$

$$\eta_p = \begin{cases} \frac{n_s}{n_p}, & TEmodes \\ \frac{n_p}{n_s}, & TMmodes \end{cases} \quad (2)$$

In equation (2), prime denotes the derivative of a function by its argument and there is an exponential

decay in the exterior solution at resonance. Given the angular mode l, a series of λ_R , ka_0andka_1values satisfy the characteristic equations (1) and (2) which are referred as the first-order mode, the second-order mode, and the third-order mode, etc. In chemical vapor sensing simulation, the increasing effective refractive index δn_p is considered and a resonance wavelength shift occurs accordingly. In the simulation modeling, the PW-HGM wall thickness has a threshold, beyond which the PW-HGM model can be simplified as a solid porous glass sphere to achieve the highest sensitivity and the best sensing characteristics. When $h > h_0$, WGMs are mainly confined inside the porous wall, and the characteristic equation of PW-HGM can be simplified to be the same as solid glass sphere characteristic equation, thus, the PW-HGM can be simplified to an ideally homogenous porous silica microsphere of radius a_1 and refractive index $n_s = n_p = 1.45$, as shown in figure 1 (a).

Chemical Vapor SensingModeling

The effective RI changes sensitivity at the interface of the microresonator and surroundings can be given by (Teraoka & Arnold, 2006; Teraoka & Arnold, 2006; Teraoka & Arnold, 2003; Lin et al., 2010):

$$S = \frac{\delta\lambda_R}{\delta n} = -\frac{\lambda_R}{\delta n}\cdot\frac{\delta k}{k_0}$$

$$\delta n = \begin{cases} \delta n_0, & Solidglasssphere \\ \delta n_p, & PW-HGM \end{cases} \quad (3)$$

For solid glass microsphere, different forms of $\delta k/k$ is given in TE and TM modes respectively (Teraoka & Arnold, 2006; Teraoka & Arnold, 2006; Teraoka & Arnold, 2003):

$$\left(\frac{\delta k}{k}\right)_{TE} = -\frac{\delta(n_0^2)\int_0^\infty T_0^2(r)dr}{2\int_0^\infty [n(r)T_0^2(r)]dr}$$

$$\left(\frac{\delta k}{k}\right)_{TM} = -\frac{\delta(n_0^2)\left[-T_0(a_0)T_0'(a_0^+) + n_0^2k_0^2\int_{a_0}^\infty T_0^2(r)dr\right]}{2n_0^4k_0^2\int_0^\infty T_0^2(r)dr}$$

$$n(r) = \begin{cases} n_s, & r < a_0 \\ n_0, & r > a_0 \end{cases}$$

$$T_0(r) = \begin{cases} \psi_l(n_s kr), & r < a_0 \\ D_l\chi_l(n_0 kr), & r > a_0 \end{cases}$$

$$D_l = \psi_l(n_s ka_0)/\chi_l(n_0 ka_0)$$

$$\delta(n_0^2) \approx 2n_0\delta n_0, \quad when\ \delta(n_0^2) \ll 1 \quad (4)$$

Using equation (4) in the equation (3), the sensitivity can thus be expressed as (Teraoka & Arnold, 2006; Teraoka & Arnold, 2006; Teraoka & Arnold, 2003; Lin et al., 2010):

$$(S_0)_{TE} = \frac{n_0\lambda_R I_0}{n_s^2 I_s + n_0^2 I_0}$$

$$(S_0)_{TM} = \frac{\lambda_R^2[n_0k_0I_0 - D_l^2\chi_l(n_0k_0a_0)\chi_l'(n_0ka_0)]}{2\pi n_0^2(I_s + I_0)}$$

$$I_s = \int_0^{a_0}[\psi_l(n_s k_0 r)]^2 dr$$

$$I_0 = \int_{a_0}^\infty [D_l\chi_l(n_0k_0r)]^2 dr \quad (5)$$

Compared to solid glass microsphere, the PW-HGM shows a more complicated form as the RI of the porous silica shell with thickness h of should be considered. Thus the forms of $\delta k/k$ in TE and TM modes are shown as (Teraoka & Arnold, 2006; Teraoka & Arnold, 2006; Teraoka & Arnold, 2003; Lin et al., 2010):

$$\left(\frac{\delta k}{k}\right)_{TE} = -\frac{\delta(n_p^2)\int_{a_0}^{a_1} T_0^2(r)dr}{2\int_0^\infty [n(r)T_0^2(r)]dr}$$

$$\left(\frac{\delta k}{k}\right)_{TM} = -\frac{\delta(n_0^2)\left[T_0'(a_1)T_0'(a_0^-) - T_0(a_0)T_0'(a_0^+) + n_p^2k_0^2\int_{a_0}^\infty T_0^2(r)dr\right]}{2n_p^4k_0^2\int_0^\infty T_0^2(r)dr}$$

$$n(r) = \begin{cases} n_s, & r < a_0 \\ n_p, & a_0 < r < a_1 \\ n_0, & r > a_1 \end{cases}$$

$$T_0(r) = \begin{cases} A_l\psi_l(n_s kr), & r < a_0 \\ B_l\psi_l(n_p kr) + \chi_l(n_p kr), & a_0 < r < a_1 \\ C_l\chi_l(n_0 kr), & r > a_1 \end{cases}$$

$$A_l = \frac{B_l\psi_l(n_p k\ a_0) + \chi_l(n_p k\ a_0)}{\psi_l(n_s k\ a_0)}$$

$$C_l = \frac{B_l\psi_l(n_p k\ a_1) + \chi_l(n_p k\ a_1)}{\chi_l(n_s k\ a_1)}$$

$$\delta(n_p^2) \approx 2n_p\delta n_p, when\ \delta(n_p^2) \ll 1 \quad (6)$$

In PW-HGM resonator, the chemical sensing equation is given using equation (3) and (6) with TE and TM modes, respectively (Teraoka & Arnold, 2006; Teraoka & Arnold, 2006; Teraoka & Arnold, 2003; Lin et al., 2010):

$$S_{TE} = \frac{n_p\lambda_R I_p}{n_s^2 I_s + n_p^2 I_p + n_0^2 I_0}$$

$$S_{TM} = \frac{\lambda_R^2\begin{bmatrix} n_s n_0 k_0 I_p + n_s C_l^2\chi_l(n_0k_0a_1)\chi_l'(n_0k_0a_1) \\ -n_0A_l^2\psi_l(n_sk_0a_0)\psi_l'(n_sk_0a_0) \end{bmatrix}}{2\pi n_s n_0 n_p(I_s + I_p + I_0)}$$

$$I_s = \int_0^{a_0}[A_l\psi_l(n_s k_0 r)]^2 dr$$

$$I_0 = \int_{a_1}^\infty [C_l\chi_l(n_0k_0r)]^2 dr$$

$$I_p = \int_{a_0}^{a_1}\left[B_l\psi_l(n_p k_0 r) + \chi_l(n_p k_0 r)\right]^2 dr \quad (7)$$

For the adsorption of chemical vapor molecules at the surface of the solid glass microsphere or into the

porous channels of the PW-HGM, the corresponding effective RI change results in the WGMs propagation optical path extension. Therefore, the TE and TM resonances shift with different wavelength range and shows diverse sensitivity response.

Experiment Design

In order to verify the theoretical sensing mechanism and demonstrate the structural variation induced sensitivity differences, a single mode fiber (SMF-28) taper coupled microresonator chemical vapor sensor is designed. A fiber taper with a length of 1 cm and a center diameter of 2 μm is fabricated from a single mode fiber (Corning SMF-28) using a fiber stretching system. The microsphere is placed in contact with the taper using a micro positioning system. Both solid glass microsphere and PW-HGM are tested separately. The experiment schematic is shown in Figure 2.

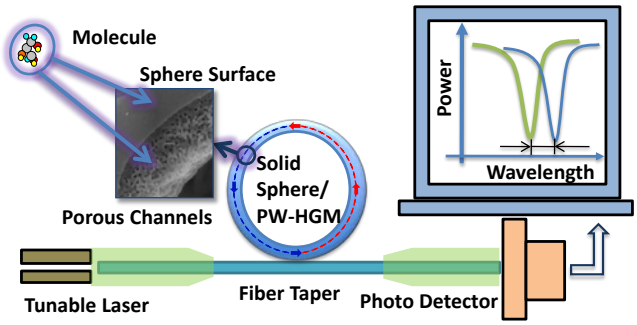

FIG. 2 SCHEMATIC OF SOLID GLASS SPHERE AND PW-HGM MICRORESONATORS IN CHEMICAL VAPOR DETECTION

In the sensing experiment, the coupling area is covered by a chamber filled with chemical vapor in different concentrations. When the solid glass microsphere or the PW-HGM is immersed into the chemical vapor environment, vapor molecules can freely interact with the microsphere surface of the solid sphere or the porous channels in the PW-HGM. Chemical vapor concentration change alters the effective index of the resonator, shifts the resonant wavelength, and be detected by a photo detector.

To demonstrate the capability of the solid glass microsphere and PW-HGM microresonator as a chemical vapor sensor, a series of experiments has been performed and various types of vapors were tested. During the experiments, the microresonator was placed in a chemical vapor chamber which was connected to the output of a bubbler placed inside an ice bath. The input bubbler was linked to a nitrogen gas tank as the carrier gas. The chemical-water solution sample was filled in the bubbler and carried by the nitrogen gas under the control of a flow meter, brought the volatized chemical from the solution sample into the chamber. The vapor concentration was varied by changing the concentration of the solution. The flow rate of the nitrogen was held constant during all experiments.

Results and Disscussions

In computational modeling, the PW-HGM modeling is demonstrated rather than the solid glass sphere. Because both types of spheres follow a similar simulation step and solid glass microsphere resonator was shown with a relatively low sensitivity compared to the PW-HGM resonator (Wang et al., 2012).

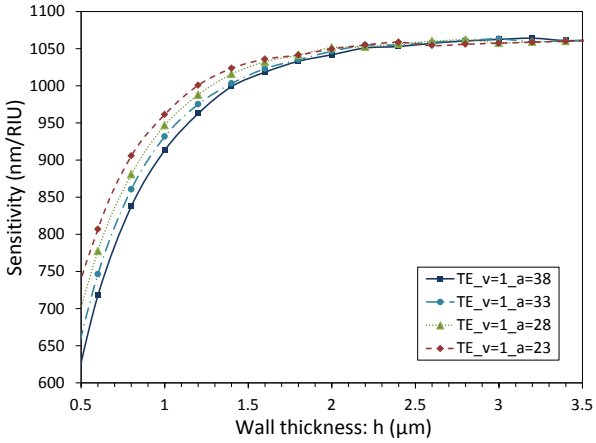

FIG. 3 THE CHEMICAL SENSITIVITY OF TE MODES IN PW-HGM RESONATOR AT DIFFERENT SPHERE SIZES AS A FUNCTION OF POROUS WALL INCREASE

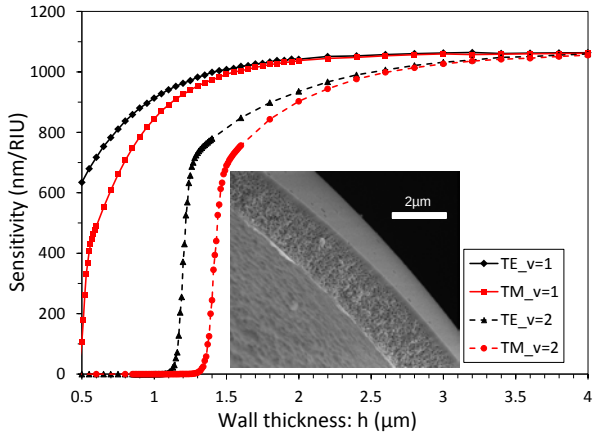

FIG. 4 PW-HGM RESONATOR CHEMICAL SENSITIVITY CHANGE AS A FUNCTION OF POROUS WALL INCREASE IN TE AND TM MODES. THE SOLID BLACK CURVE IS THE FIRST ORDER TE MODE; THE SOLID RED CURVE IS FIRST ORDER TM CURVE; THE DASHED BLACK CURVE IS SECOND ORDER TE MODE AND THE DASHED RED CURVE IS SECOND ORDER TM MODE

In the simulation, first, various sizes of PW-HGMs with different sensitivity are demonstrated. Figure 3 shows the sensitivity change of different sizes PW-HGMs resonators in the fundamental TE modes as a function of wall thickness. PW-HGMs with an increasing size are simulated with radius of 23 μm, 28

μm, 33 μm and 38 μm, respectively. The sensitivity increases as the porous wall gets thicker. The sensitivity of resonators in all sizes turns out to be in the same level when the sphere porous wall is thicker than 2 μm, which is the proposed wall thickness threshold for PW-HGM resonator model simplification in modelling section. In practice, the PW-HGM with diameter of 75 μm was tested in the experiment. Thus, the simulation focuses on this specific size and the porous wall thickness effect as well as its modes has been investigated.

Figure 4 gives the sensitivity changing trend of the 75 μm PW-HGM under different wall thicknesses in several modes. The parameter a in the figure legend is the radius of the microsphere. First-order and second-order of TE and TM modes are shown with different sensitivity. The figure demonstrates the increasing trend of sensitivity when the porous wall is getting thicker under different modes. For the first order modes, the highest increasing slope exists at the wall thickness between 1 μm and 2 μm. The sensitivity of the first order modes stabilizes when the porous wall is thicker than 2 μm. The stability of second order occurs at 3 μm. The inset of figure 4 shows the actual wall thickness of the PW-HGM. The fundamental TE and TM modes with $v = 1$ always provide a higher sensitivity compared to higher order.

In figure 4, the wall thickness in nanometer scale is considered compared to figure 3. The fundamental modes of TE and TM show a high sensitivity increase from 500 nm to 1 μm wall thickness. However, the second-order TE and TM modes do not even exist in that wall thickness range. Meanwhile, the fundamental TE mode shows a higher sensitivity than the fundamental TM mode in nano scale wall thickness. Thus, the first order TE mode of PW-HGM resonator is used to compare with the experiment.

Based on the optimization results in the theoretical part, the PW-HGM with diameter of 75 μm and wall thickness of 2 μm was used in the experiment. Chemical vapors of pure ethanol and pure acetone were tested. Figure 5 shows the different responses of the PW-HGM resonator with respect to the chemical vapor change. The increase in molecule size has led to a wider range of wavelength shift.

Based on the optimization results in the theoretical part, the PW-HGM with diameter of 75 μm and wall thickness of 2 μm was used in the experiment. Chemical vapors of pure ethanol and pure acetone were tested. Figure 5 shows the different responses of the PW-HGM resonator with respect to the chemical vapor change. The increase in molecule size has led to a wider range of wavelength shift.

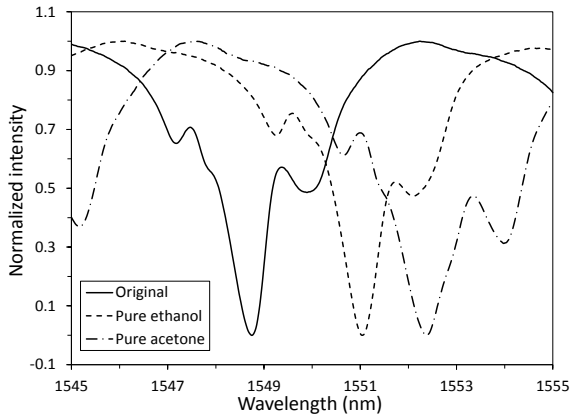

FIG. 5 PW-HGM MICRORESONATOR OPTICAL SPECTRUM IN DIFFERENT CHEMICAL VAPOR TYPES (Wang et al., 2012).

Different concentrations of acetone vapor were tested using PW-HGM microresonator. In the experiment, 1%, 5%, 10%, 25%, 50% and 100% acetone solutions were used. Compared to the environment before the acetone vapor was involved, the corresponding refractive index changes are 0.0003, 0.002, 0.0026, 0.0032, 0.0036 and 0.004, respectively. Figure 6 shows the wavelength shift of the resonance as functions of the solution concentration increase for simulation and experiment results. In low concentration of the acetone vapor under 25%, the resonant wavelength shift of the resonator increased rapidly. On the other hand, the wavelength shift became slow at higher acetone vapor concentrations. The relationship between the resonance shift and the concentration agreed qualitatively with the Langmuir adsorption model. Adsorption of varying vapor concentrations at different refractive indices may result in different amount of changes in the effective refractive index of the glass-vapor mixture. Therefore, it is expected that the sensitivity of the resonators depends on the size and polarity of the molecule.

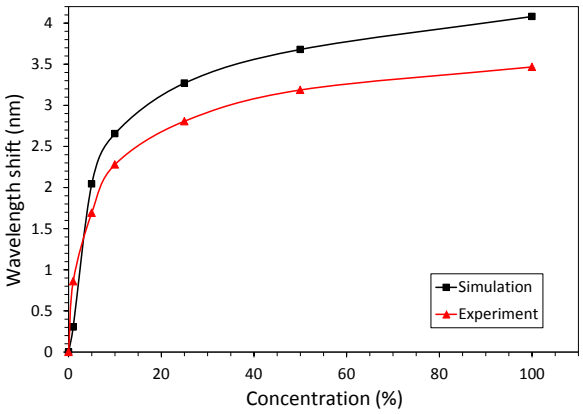

FIG. 6 SIMULATION AND EXPERIMENT OF PW-HGM RESONATOR FOR CHEMICAL VAPOR DETECTION SENSITIVITY. BLACK CURVE WITH SQUARE MARKER IS THE SIMULATION AND RED CURVE WITH TRIANGLE MARKER IS THE EXPERIMENT

From figure 6, it can be seen that the simulation results agree well with the sensitivity increasing trend of the experiment data. The reason for a lower sensitivity in the experiment is because acetone vapor may be diluted during the storage or transmission stage.

Conclusions

In summary, a chemical vapor sensor using glass microsphere as the optical resonator was investigated theoretically and experimentally. Computational model revealed that the essence of molecular adsorption caused refractive index change on the sphere surface of a solid glass sphere and through the porous channels of a PW-HGM. The adsorption of chemical vapor molecules into the nano-sized pores in the wall of the PW-HGM enhanced the change in the effective refractive index of the material, causing a shift in the resonance spectrum towards longer wavelengths. The vapor concentration enhancement increased the amount of wavelength shift. The computational simulation agreed well with the experimental results in the sensing trend. It is expected that the experimentally verified optical microresonator model can be used for prediction and optimization of the resonator for high sensitive chemical vapor detection.

ACKNOWLEDGMENT

This research work was supported by research funding provided by U.S. Army Research Office (ARO) under contract: W911NF-10-2-0077.

REFERENCES

Crone, B., Dodabalapur, A., Gelperin, A., Torsi, L., Katz, H. E., Lovinger, A. J., et al., "Electronic sensing of vapors with organic transistors," Applied Physics Letters, 78, 15 (2001), 2229-31.

Crone, B. K., Dodabalapur, A., Sarpeshkar, R., Gelperin, A., Katz, H. E., and Bao, Z., "Organic oscillator and adaptive amplifier circuits for chemical vapor sensing," Journal of Applied Physics, 91, 12 (2002), 10140-6.

Gregor, M., Pyrlik, C., Henze, R., Wicht, A., Peters, A., and Benson, O., "An alignment-free fiber-coupled microsphere resonator for gas sensing applications," Applied Physics Letters, 96, 23 (2010), 231102-4.

Homola, J., Yee, S. S., and Gauglitz, G., "Surface plasmon resonance sensors: review," Sensors and Actuators, B: Chemical, 54, 1 (1999), 3-15.

Lin, N., Jiang, L., Wang, S., Yuan, L., Xiao, H., Lu, Y., et al., "Ultrasensitive chemical sensors based on whispering gallery modes in a microsphere coated with zeolite," Applied Optics, 49, 33 (2010), 6463-71.

Matsko, A. B., and Ilchenko, V. S., "Optical resonators with whispering-gallery modes - Part I: Basics," IEEE Journal on Selected Topics in Quantum Electronics, 12, 1 (2006), 3-14.

Patrick, H. J., Kersey, A. D., and Bucholtz, F., "Analysis of the response of long period fiber gratings to external index of refraction," Journal of Lightwave Technology, 16, 1 (1998), 1606-12.

Teraoka, I., and Arnold, S., "Theory of resonance shifts in TE and TM whispering gallery modes by nonradial perturbations for sensing applications," Journal of the Optical Society of America B: Optical Physics, 23, 7 (2006), 1381-9.

Teraoka, I., Arnold, S., and Vollmer, F., "Perturbation approach to resonance shifts of whispering-gallery modes in a dielectric microsphere as a probe of a surrounding medium," Journal of the Optical Society of America B: Optical Physics, 20, 9 (2003), 1937-46.

Teraoka, I., and Arnold, S., "Enhancing the sensitivity of a whispering-gallery mode microsphere sensor by a high-refractive-index surface layer," Journal of the Optical Society of America B: Optical Physics, 23, 7 (2006), 1434-41.

Wang, H., Yuan, L., Kim, C. W., Han, Q., Wei, T., Lan, X., and Xiao, H., "Optical microresonator based on hollow sphere with porous wall for chemical sensing," Optics Letters, 37, 1 (2012), 94-6.

Wan, Q., Li, Q. H., Chen, Y. J., Wang, T. H., He, X. L., Li, J. P., et al., "Fabrication and ethanol sensing characteristics of ZnO nanowire gas sensors," Applied Physics Letters, 84, 18 (2004), 3654-6.

Wei, C., Dai, L., Roy, A., and Tolle, T. B., "Multifunctional chemical vapor sensors of aligned carbon nanotube and polymer composites," Journal of the American Chemical Society, 128, 5 (2006), 1412-3.

Zamborini, F. P., Leopold, M. C., Hicks, J. F., Kulesza, P. J., Malik, M. A., and Murray, R. W., "Electron hopping conductivity and vapor sensing properties of flexible network polymer films of metal nanoparticles," Journal of the American Chemical Society, 124, 30 (2002), 8958-64.